Mechanical, Electrical and Electro-Mechanical Properties of Thermoplastic Elastomer Styrene-Butadiene-Styrene/Multiwall Carbon Nanotubes Composites

P. Costa[1], J. Silva[1,2], V. Sencadas[1,3], R. Simoes[2,3], J. C. Viana[2], S. Lanceros-Méndez[1,*]

1- Centro/Dept. de Física da Universidade do Minho, 4710-058 Braga, Portugal

2- Institute for Polymers and Composites IPC/I3N, University of Minho, 4800-058 Guimarães, Portugal

3- School of Technology, Polytechnic Institute of Cávado and Ave, Campus do IPCA, 4750-810 Barcelos, Portugal.

*lanceros@fisica.uminho.pt; tel: + 351 253 604073; fax: + 351 253 253604061

Abstract

Composites of styrene-butadiene-styrene (SBS) block copolymer with multiwall carbon nanotubes (MWCNT) were processed by solution casting in order to investigate the influence of filler content, the different ratio of styrene/butadiene in the copolymer and the architecture of the SBS matrix on the electrical, mechanical and electro-mechanical properties of the composites. It was found that filler content and elastomer matrix architecture influence the percolation threshold and consequently the overall composite electrical conductivity. The mechanical properties are mainly affected by the styrene and filler content. Hopping between nearest fillers is proposed as the main mechanism for the composite conduction. The variation of the electrical resistivity is linear with the deformation. This fact, together with the gauge factor values in the range of 2 to 18, results in appropriate composites to be used as (large) deformation sensors.

Keywords: Functional composites; Polymer-matrix composites; Electrical properties; Elastic properties; Piezoresistive Sensors

1 Introduction

Elastomers and thermoplastics are known for their capability to exhibit high deformation capability and high electrical and thermal resistances [1]. These properties can be significantly modified by the addition of conductive fillers such as carbon allotropes [1]. Within this family, carbon nanotubes (CNT) are known to produce composites with superior electrical and mechanical properties compared with other carbon allotropes such as carbon black (CB) or carbon nanofibers (CNF) [1]. The CNT unique electrical and mechanical properties [2] allows that even at low concentrations (less than 5 wt%) they can strongly affect the composite's electrical and mechanical properties [3-4].

Thermoplastic elastomer tri-block copolymer styrene-butadiene-styrene (SBS) copolymers can be composed by different ratios of styrene and butadiene, influencing strongly their macroscopic properties.

The application range of SBS, once suitably reinforced with CNT, can be extended to a variety of products such as sensors and actuators [5], materials with electromagnetic shielding properties [6], vapour and infrared sensors [7] and capacitors [8], among others. Previous studies on SBS – carbon nanotube composites indicate that the final properties of the composite can change for different ratios of styrene and butadiene [9].

Despite the intensive use of SBS in industry, the potential of SBS/CNT nanocomposites for sensor applications has been scarcely explored and systematic studies on the interrelationship of styrene/butadiene ratio and CNT loading on the electrical, mechanical and electro-mechanical response, have yet to be done.

The composites using CNT show higher enhancement in the electrical properties that can be interpreted within the framework of percolation theory [10-11]. The percolation

theory predicts for fibres with a capped cylinder shape the following bounds for the percolation threshold [10], [12]::

$$1-e^{\frac{-1.4V}{\langle V_e \rangle}} \leq \Phi_c \leq 1-e^{\frac{-2.8V}{\langle V_e \rangle}} \quad (1)$$

Equation 1 links the average excluded volume $\langle V_e \rangle$,i.e., the volume around an object in which the centre of another similarly shaped object is not allowed to penetrate, averaged over the orientation distribution, with the critical concentration (Φ_c). Here, 1.4 corresponds to the lower limit for infinitely thin cylinders and 2.8 correspond to spheres (V is the particle volume). For high aspect ratio fillers the percolative network can be formed with lower concentrations producing a composite with higher electrical and mechanical properties. The percolation threshold found for this type of nanocomposites depends on the properties of the materials (matrix and nanoparticles) [13], nanofiller dispersion agent and method [14] and can be reduced down to 0.1 % volume using CNT [1]. The typical percolation threshold is between 10-25 % volume for CB [1] and 1-5 % volume to CNF [1].

An important property of CNT/polymer composites that can be used for sensor applications is the fact that by the application of uniaxial or hydrostatic stress, the composite electrical resistivity changes, due to the so called piezoresistance [15]. It is important to note that this change on the composite electrical resistivity due to the applied stress is not solely related to changes in the dimension of the solid or to the intrinsic piezoresistance of the components. The piezoresistivity in CNT/polymer composites can be mainly attributed to the variations of the conductive networks with strain, such as loss of contact between the fillers, tunnelling effect in neighbouring fillers and conductivity change due to the deformation of CNT [15]. It is also known that, even for the same kind of carbon allotrope, the piezoresistance effect is highly

dependent on the physical and chemical properties of the filler [16]. The piezoresistance effect of CNT/polymer composites makes them particularly interesting materials to be used as highly sensitivity strain sensors for structural health monitoring [17], damage and fracture detection [18]. In particular, elastomeric based composites are exceptionally appropriate for high strain and high compliant deformation sensors, due to the difficulties of other materials in achieving high level reversible deformations.

The piezoresistive effect results from the strain-induced variation of the electrical resistance of the material. At low strains, in thermoplastic elastomer/CNT composites, the resistance changes linearly with strain. This linearity is sometimes referred as Gauge Factor, *Gf* [19]:

$$Gf = \frac{\Delta R / R_0}{\varepsilon} \tag{2}$$

where, ε is the strain and $\Delta R / R_0$ is the factional electrical resistance change with the strain.

In the present work, SBS/MWCNT composites were processed by solution casting for different styrene/butadiene ratios and matrix architecture (radial and linear), as well for different filler loadings. The influence of these parameters on the mechanical and electrical response of the material was studied as well as their electro-mechanical performance through the calculation of the Gauge Factor. In this way, the fundamental properties concerning the electrical and mechanical performance of the material were discussed, as well as its potential for use in large strain sensor applications.

2 Experimental

Commercial Calprene C401, C411, C500 and 540 tri-block copolymer of styrene-butadiene-styrene (SBS) with the properties presented in Table 1 were supplied by Dynasol Gestión, S.A (Spain). High purity multi-walled carbon nanotubes (MWCNT, Baytubes C 150P; purity > 95%, outer mean diameter = 13–16 nm, and length = 1– > 10 μm) were supplied by Bayer Materials Science, Germany. The SBS copolymers were employed with tree different ratios of styrene and butadiene and two different structures (radial and linear block copolymers).

For the preparation of the nanocomposites, MWCNT were placed in an Erlenmeyer with toluene and kept in an ultrasound bath (*Bandelin*, Model Sonorex Super RK106) for 6 h to promote a good dispersion of the MWCNT. After this stage, SBS was added to the solution and stirred until complete dissolution was achieved. The relation of SBS to toluene is 1 g for 5.5 ml. Thin and highly flexible composites films were obtained by spreading the solution on a clean glass substrate. The evaporation of toluene was performed at room temperature. MWNT dispersion and distribution in the polymer matrix was evaluated by scanning electron microscopy (SEM) with a SEM Phillips X230 FEG apparatus. Cross section images were obtained after cutting the samples previously immersed in liquid nitrogen and coating the surface gold using a sputter coating.

The variation of the electrical resistance of the samples was calculated from the slope of I–V curves measured with an automated Keithley 487 picoammeter/voltage source. I–V data points were collected in ~0.3 mm thick samples between 5 mm diameter Au contacts previously deposited with a Polaron SC502 sputter coater. The applied voltage ranged between − 10 V and + 10 V. The volume resistivity of the samples (ρ) was calculated by:

$$\rho = \frac{RA}{d} \tag{3}$$

where, R is the measured electrical resistance, A is the electrode area and d is the thickness of composites. The electrical conductivity (σ) in Sm^{-1} was calculated from the inverse of ρ as the average of three measurements.

Mechanical measurements were performed on rectangular samples with an area of about 60 mm x 20 mm using an AG-IS universal testing machine from Shimadzu with load cell of 1 KN in tensile mode at a test velocity of 1 mm/min and at room (~23 ºC) temperature. The mechanical parameters were obtained as the average of three measurements. The piezoresistive effect was calculated by mechanical stress-strain tests and measuring in real-time the electrical resistance of the sample in a digital multimeter (6½ digit), Agilent 34401A. The surface electrical resistance was measured by placing electrodes in the clamps of the tensile machine. In this case, the electrodes do not suffer any deformation, therefore maintaining a constant area. The distance between electrodes is equal to the grip distance, measured by the tensile machine.

3 Results and Discussion

3.1 MWCNT dispersion

SEM images of SBS/MWCNT composites for the C540 matrix with 1% and 4% of MWCNT are presented in figure 1 for two magnifications. Similar images are observed for the different polymer matrices. The samples are characterized by small MWCNT clusters well dispersed in the different SBS matrix. Therefore, composites with some degree of agglomeration of the nanotubes are obtained, but with a relatively good cluster distribution. This fact is independent of the polymer matrix.

3.2 Mechanical Properties

Representative quasi-static stress/strain curves for the different SBS matrices are presented in figure 2. The materials undergo yielding and strain hardening as the strain increases. A first maximum stress is observed for all samples followed by a post-yielding plateau and a strain hardening stage before the rupture of the material. The stress-strain curves of figure 2 reveal that the SBS with radial morphology has lower tensile strength and presents a strain at rupture of approximately 1100 %. On the other hand, the SBS with linear morphology shows higher tensile strength. The highest strain at rupture (~ 1400%) is found for the sample C540, which has a linear structure and the higher amount of the styrene in its composition (40%). The linear morphology SBS leads to higher strain-hardening modulus. It is also observed for both types of SBS architectures that the maximum sustained stress level of the SBS increases with increasing styrene content in the copolymer.

It has been reported that the deformation induced in the SBS block copolymer depends strongly on the morphology and microdomain orientation [20]. In principle, the solution cast films do not have any preferable molecular orientation. During stretching, the orientation of the macromolecular chains and individual phases along the draw direction plays an important role in the material deformation. A linear architecture of the block copolymer allows also a higher material stretchability rather than a radial one. In figure 2, the initial moduli of the neat SBS matrices are substantially higher for linear architecture and for a high amount of styrene. The amount of styrene present in the copolymer increases the sustained stress level of the material, especially for the samples with linear structure (C500 and C540). The measured stress at 300 % of strain (σ_{300}) and

at 900 % of strain (σ_{900}) reveal that σ_{300} and σ_{900} increases with the increasing amount of PS present in the sample and it is also higher for the material with linear morphology (figure 2).

Figure 3a) shows the stress-strain curves for C540 SBS (the matrix showing the highest elastic modulus and deformation at break) / MWCNT composites with filler volume fractions up to 3.83×10^{-2}. For low filler volume fractions (up to 9.87×10^{-3}) increasing MWCNT content increases slightly the strain hardening response of the material without compromising its deformation capabilities (figure 3a). However, for higher MWCNT contents the strain hardening is substantially reduced, still without reducing the maximum strain at break. Table 2 presents the main mechanical properties of the C540 SBS/ MWCNT composites. It is also observed that the initial modulus increases with increasing MWCNT content, suggesting a good adhesion between the SBS and the MWCNT. The σ_{300} values are quite similar for all samples, suggesting that the MWCNTs are homogeneous and uniformly dispersed into the polymer matrix. This is further corroborated by the small variation of the strain at break with increasing MWCNT content. Finally, the ultimate tensile strength increases for small amounts of nanofiller added to the SBS until 1.95×10^{-2} volume fraction, decreasing slightly for higher filler concentrations.

The inclusion of MWCNT into the polymer matrix leads to an increase in the elastic modulus, which is a common behaviour of this kind of polymeric systems [16]. It should be noted that the strength is almost similar for all samples until $\varepsilon \sim 700\%$, but for the sample with 3.83×10^{-2} filler volume fraction, the tensile stress is smaller than the ones found for the composite samples with lower filler contents. The formation of MWCNT aggregates in the polymer composite [14] represent a common defect that for

higher strains explains the decrease of the tensile tress for the sample with highest filler content. The retaining of the tensile strength observed in the samples suggests the presence of just small extent of agglomerates (table 2).

In order to understand the effect of the MWCNTs into the different SBS morphologies, several samples were processed with 1.95-3.68x10^{-2} filler volume fractions. Figure 3b) shows the stress-strain curves indicating that all SBS nanocomposites show the same deformation trends. The C540 matrix (with linear SBS architecture and high styrene content) filled with 1.95x10^{-2} volume fraction of MWCNT shows the best mechanical performance, namely the highest sustained stresses. The C500 matrix (with linear SBS architecture and low styrene content) presents the lowest stress levels. The C411 matrix (with radial SBS architecture and high styrene content) shows the highest strain hardening slope. The architecture type and the styrene content in the SBS matrix have distinct effects on the mechanical response of the SBS/MWCNT composites.

Comparing with the neat SBS stress-strain curves (Figure 3a) the incorporation of MWCNT improves the mechanical response of the SBS matrices. In general, the initial modulus increases significantly, showing linear SBS nanocomposites lower initial modulus when compared to the radial ones. Increasing styrene content leads to higher initial modulus of the nanocomposites. For the radial SBS morphologies, the ultimate stress increases significantly with the incorporation of the fillers, but for the linear SBS, adding the nanofillers reduces the maximum stress level. As already mentioned, the initial modulus of the SBS nanocomposites dependen upon the copolymer morphology (radial vs. linear) and the styrene content on the SBS.

Figure 4 shows the variation of the initial modulus of the SBS systems with the MWCNT content. For a given SBS matrix, E increases with increasing filler content. The elastic modulus are higher for the C540 samples due to the larger styrene (40%)

content , leading to a stiffer material. Conversely the C401 sample shows the lowest E values. Finally, comparing similar styrene/butadiene ratios, C411 and C500, the initial modulus is larger for the SBS with a radial structure, C411, than that with a linear structure, C500, and this behaviour is correlated to the distribution and uniformity of the styrene phase among the copolymer.

3.3 Electrical Properties

The electrical response of the SBS/MWCNT composites was evaluated by measuring the bulk electrical resistivity (figure 5a).

Figure 5a) shows the electrical conductivity of the SBS nanocomposites as a function of the volume fraction of MWCNT. For C401, C411 and C500 nanocomposites there is a critical volume fraction were a change of several orders of magnitude in the electrical conductivity is observed. For the C540, the position of the critical volume fraction is not clear, but a sharp increase in the electrical conductivity is observed, leading to a quasi-plateau for the highest volume fractions. The electrical conductivity seems to be also dependent on the morphology and styrene content of the SBS block copolymers. Interestingly, the variations of the electrical conductivity for the SBS nanocomposites are similar to those of the initial modulus. The C540 shows the highest values of the initial modulus and electrical conductivity, followed by C411, C500; the C401 showing the lowest values. In this way, the electrical conductivity of the nanocomposites, such as the modulus, is also dependent upon the copolymer morphology (radial vs. linear) and the styrene content.

In fact, as the same type of MWCNT are used for all composites, the matrix characteristics should also be used to explain the observed differences in the electrical

behaviour. Together with the fibre characteristics (e.g., size, aspect ratio), typically taken into account by different theoretical models, the range of the matrix-mediated interactions between the fillers has also to be considered [21]. The percolation threshold, Φ_c, depends also upon the type of matrix [21]:

$$\Phi_c = \frac{D^2}{2L\delta_{\max}} \tag{4}$$

where, D is the MWCNT outer diameter, L their length and δ_{max} is related to the maximum interaction range between two adjacent MWCNT (matrix dependent) [22]. Usually, the length of the MWCNT is not uniform, exhibiting a length distribution. Assuming that this distribution can be described by a Gaussian distribution with an average length L_{av} and a variance σ^2, the effect of the MWCNT length distribution in the percolation threshold can be studied by substituting the length by an weighted average length $\langle L \rangle_w$ in Equation (4) [22], leading to:

$$\Phi_c = \frac{D^2}{2\langle L \rangle_w \delta_{\max}} \tag{5}$$

with $\langle L \rangle_w \propto L_{av} + \frac{\sigma^2}{L_{av}}$, where L_{av} is the average MWCNT length. Usually the electrical conductivity of the composites is understood within the percolation theory, which predicts a power law dependence for the electrical conductivity, σ, upon the volume fraction of conductive particles, valid for $\Phi \geq \Phi_c$, and expressed by:

$$\sigma \propto \left(\Phi - \Phi_c\right)^t \tag{6}$$

where, *t* is a universal critical exponent depending only on the system dimension, Φ is the volume fraction and Φ_c is the critical concentration at which an infinite cluster appears in the composite [21]. Using equation (6), the percolation threshold and the critical exponent were calculated for all composites, with the exception of the C540,

were the fits were inconclusive. Further, the maximum interaction range (δ_{max}) was established using Equation 5 with the average values for the MWCNT diameter and length presented in the Experimental section and assuming that $\sigma = \frac{L_{av}}{2}$ is equal for all composites. It was also assumed that the value for the standard deviation is the same for all composites due to the fact that all MWCNT came from the same batch and that the processing conditions for the preparation of the nanocomposites were the same. It is also important to note that MWCNT aggregate into clusters and, therefore, MWCNT clusters must be considered as conductivity units, comprised of several individual MWCNT with a given effective length. The latter reasoning leads to choose large values for the length standard deviation (table 3).

It can be concluded from Table 3 that the percolation threshold, Φ_c, decreases with the addition of styrene (C401 and C411). Furthermore, for composites with the same ratio of styrene/butadiene (C411, C500) the percolation threshold is lower for SBS with a linear structure (C500) as compared to those with a radial one (C411). It is also observed that the lower percolation threshold implies that δ_{max} is higher, this meaning a higher interaction range between two MWCNT for a specific matrix. The high percolation threshold observed for the radial SBS structure can be attributed to electrostatic screening by the radial structures, lowering the maximum effective interaction distance between two MWCNT and therefore increasing the percolation threshold.

In Table 3, the critical exponents, t, for the power law described by Equation 6 are also shown. A wide range of values for the critical exponents were found: the C401 composites have a value typical of a Bethe lattice [21], the C411 has the electrical mean field approximation value [11] and the critical exponent for the C500 has the typical

value of a 3D system [21].The fact that the expected power law value predicted by the percolation theory was found within a wide range of values leads to consider that, indeed, there exists a giant component that spans the system, but that the conduction mechanism can be attributed to a matrix mediated hopping leading to a weak disorder regime [19-20]. This weak disorder regime can be described by:

$$G_{eff} = G_{cut} \exp\left(\frac{-l_{opt}}{\left(N_{\max}\Phi\right)^{1/3}} \right) \tag{7}$$

were, l_{opt} is the length of the optimal path. When most of the links of the path contribute to the sum, the system is said to be in the "weak disorder" regime [23]. Conversely, the case where a single link dominates the sum along the path is called the "strong disorder" limit [23]. In Equation 7, N_{max} is the maximum number of fillers in the domain and G_{cut} is the effective electrical conductance of the system before a bond with maximum conductance is added to (or removed from) the system [23]. The l_{opt} parameter is related to the disorder strength when the system is in the weak disorder regime. The disorder strength is just the inverse of the scale over which the wave function decays in the polymer (x_0), as expressed by the hopping conductivity expression at room temperature [24-25]:

$$\sigma_{ij} = \sigma_0 \exp\left(-\frac{x_{ij}}{x_0}\right) \tag{8}$$

where σ_0 is the dimension coefficient and x_{ij} is the distance between two fillers. As described in [26], applying Equation 8 to the gap between the fillers (described as the minimum distance between two rods) and thus defining the electrical conductivity by hopping between adjacent fillers, leads to Equation 7. This agrees well with recent results [26], which demonstrate that hopping between adjacent fillers gives rise to the expression $\log(\sigma) \propto \Phi^{-\frac{1}{3}}$, as given by Equation (7), which corresponds to a weak

disorder regime. This relation is also found in fluctuation-induction tunnelling [27] for the DC conductivity. In order to prove the latter assumptions, the $\log(\sigma) \propto \Phi^{-1/3}$ dependence was tested for all composites (Figure 5b).

Figure 5b shows that there is a linear relation between the logarithm of the electrical conductivity and the volume fraction of MWCNT (with a $R^2 > 0.9$). It is important to note that for the SBS C401, C411 and C500 matrices there is a deviation from the linear relation for the lower MWCNT volume fractions, indicating that the conductive network is not yet formed, and implying that $G_{eff} = G_{cut}$ [26], i.e., the effective electrical conductance is controlled by the matrix conductance. On the other hand, for the C540 nanocomposite there are also deviations from the linear relationship for the higher volume fractions, which may be explained by the earlier formation of a spanning cluster [21]. For the C540 composite the spanning cluster is established at lower filler volume fractions (Figure 5b), which implies that increasing MWCNT content does not further contribute to the overall composite electrical conductivity. Hopping between nearest fillers leads to the deviation from the percolation theory and the overall nanocomposite electrical conductivity is explained by the existence of a weak disorder regime.

3.4 Electro-mechanical Properties

The piezoresistive effect was assessed for the SBS/MWCNT nanocomposites in the strain range between 5 to 20% in order to test the suitability of these materials for strain sensor applications. The measurements were performed in composites with volume fractions just above the percolation threshold in order to maintain suitable resistance values to be measured as large stretching is applied (i.e., at volume fractions of $1.95 \times 10^{-}$

^{2}). The obtained GF ranges from 2 to 18, the highest values being obtained for the composite C540 at 20% strain (Figure 6b).

In Figure 6a) are presented the variations of the electrical resistance with a reversible strain loading (loading and unloading cycles). The relationship is linear and the electrical resistance increases with the deformation. This fact, together with the large values obtained for the GF, indicates the suitability of these nanocomposites for high strain deformation sensors.

Figure 6b) shows the variation of GF with strain for the C540 matrix. GF increases with increasing strain. There are still no consolidated theories explaining piezoresistivity in conducting particle-reinforced insulating matrix composites. Theories for the GF based on elastic heterogeneity, where the conducting phase is stiffer than the insulating one, indicate that the local strains within the latter are higher with respect to the averaged macroscopic strains, thus inducing higher GF values [28]. In this case, the increase of the GF with increasing strain is ascribed to larger induced variations in the conductive network due to larger induced local strains on the matrix.

Conclusions

SBS/MWCNT composites were processed by solution casting with different MWCNT contents. It was found that both the architecture of the block copolymer elastomer (i.e., radial vs linear) and the styrene/butadiene ratio influence the electrical conductivity of the SBS/MWCNT composites. Conversely, regarding the mechanical properties, the influence of the SBS architecture was not observed, with the mechanical response being dominated by the styrene/butadiene ratio. Hopping between nearest fillers is the main mechanism for the composite electrical conduction; the overall composite conductivity

is explained by the existence of a weak disorder regime. Finally, the obtained values for the Gauge Factor reveal the potential of these materials for large strain sensor applications.

Acknowledgements

This work was funded by FEDER funds through the "Programa Operacional Factores de Competitividade – COMPETE" and by national funds by FCT - Fundação para a Ciência e a Tecnologia, through project references PTDC/CTM/69316/2006, PTDC/CTM/73465/2006, PTDC/CTM-NAN/112574/2009, and NANO/NMed-SD/0156/2007. PC, JS and VS also thank FCT for the SFRH/BD/64267/2009, SFRH/BD/60623/2009 and SFRH/BPD/63148/2009 grants, respectively. The authors also thank support from the COST Action MP1003 ”European Scientific Network for Artificial Muscles” and the COST action MP0902 “Composites of Inorganic Nanotubes and Polymers (COINAPO)”

References

[1] Lorenz H, Fritzsche J, Das A, Stöckelhuber KW, Jurk R, Heinrich G, et al. Advanced elastomer nano-composites based on CNT-hybrid filler systems. Composites Science and Technology. 2009;69(13):2135-2143.

[2] J-H. Du, J. Bai, Cheng H-M. The present status and key problems of carbon nanotube based polymer composites. Express Polymer Letters. 2007;1(5):253-273.

[3] Ma P-C, Siddiqui NA, Marom G, Kim J-K. Dispersion and functionalization of carbon nanotubes for polymer-based nanocomposites: A review. Composites Part A: Applied Science and Manufacturing. 2010;41(10):1345-1367.

[4] Sahoo NG, Rana S, Cho JW, Li L, Chan SH. Polymer nanocomposites based on functionalized carbon nanotubes. Progress in Polymer Science. 2010;35(7):837-867.

[5] De Falco A, Goyanes S, Rubiolo GH, Mondragon I, Marzocca A. Carbon nanotubes as reinforcement of styrene-butadiene rubber. Applied Surface Science. 2007;254(1):262-265.

[6] Koerner H, Liu W, Alexander M, Mirau P, Dowty H, Vaia RA. Deformation-morphology correlations in electrically conductive carbon nanotube--thermoplastic polyurethane nanocomposites. Polymer. 2005;46(12):4405-4420.

[7] Li C, Thostenson ET, Chou T-W. Sensors and actuators based on carbon nanotubes and their composites: A review. Composites Science and Technology. 2008;68(6):1227-1249.

[8] Tsuchiya K, Sakai A, Nagaoka T, Uchida K, Furukawa T, Yajima H. High electrical performance of carbon nanotubes/rubber composites with low percolation threshold prepared with a rotation-revolution mixing technique. Composites Science and Technology. 2011;71(8):1098-1104.

[9] Pedroni LG, Soto-Oviedo MA, Rosolen JM, Felisberti MI, Nogueira AF. Conductivity and mechanical properties of composites based on MWCNTs and styrene-butadiene-styrene block™ copolymers. Journal of Applied Polymer Science. 2009;112(6):3241-3248.

[10] Celzard A, McRae E, Deleuze C, Dufort M, Furdin G, Marêché JF. Critical concentration in percolating systems containing a high-aspect-ratio filler. Physical Review B. 1996;53(10):6209-6214.

[11] Kirkpatrick S. Percolation and Conduction. Reviews of Modern Physics. 1973;45(4):574-588.

[12] Balberg I, Anderson CH, Alexander S, Wagner N. Excluded volume and its relation to the onset of percolation. Physical Review B. 1984;30(7):3933-3943.

[13] Silva J, Ribeiro S, Lanceros-Mendez S, Simões R. The influence of matrix mediated hopping conductivity, filler concentration, aspect ratio and orientation on the electrical response of carbon nanotube/polymer nanocomposites. Composites Science and Technology. 2011;71(5):643-646.

[14] Wang P, Geng S, Ding T. Effects of carboxyl radical on electrical resistance of multi-walled carbon nanotube filled silicone rubber composite under pressure. Composites Science and Technology. 2010;70(10):1571-1573.

[15] Taya M, Kim WJ, Ono K. Piezoresistivity of a short fiber/elastomer matrix composite. Mechanics of Materials. 1998;28(1-4):53-59.

[16] Paleo AJ, Hattum FWJv, Pereira J, Rocha JG, Silva J, Sencadas V, et al. The piezoresistive effect in polypropylene—carbon nanofibre composites obtained by shear extrusion. Smart Materials and Structures. 2010;19(6):065013.

[17] Kang I, Heung YY, Kim JH, Lee JW, Gollapudi R, Subramaniam S, et al. Introduction to carbon nanotube and nanofiber smart materials. Composites Part B: Engineering. 2006;37(6):382-394.

[18] Thostenson ET, Chou TW. Carbon Nanotube Networks: Sensing of Distributed Strain and Damage for Life Prediction and Self Healing. Advanced Materials. 2006;18(21):2837-2841.

[19] Oliva-Avilés AI, Avilés F, Sosa V. Electrical and piezoresistive properties of multi-walled carbon nanotube/polymer composite films aligned by an electric field. Carbon. 2011;49(9):2989-2997.

[20] Huy TA, Adhikari R, Michler GH. Deformation behavior of styrene-block-butadiene-block-styrene triblock copolymers having different morphologies. Polymer. 2003;44(4):1247-1257.

[21] Stauffer D, Aharony A. Introduction to percolation theory. London1992.

[22] Kyrylyuk AV, van der Schoot P. Continuum percolation of carbon nanotubes in polymeric and colloidal media. Proceedings of the National Academy of Sciences. 2008;105(24):8221-8226.

[23] Sreenivasan S, Kalisky T, Braunstein LA, Buldyrev SV, Havlin S, Stanley HE. Effect of disorder strength on optimal paths in complex networks. Physical Review E. 2004;70(4):046133.

[24] Ambegaokar V, Halperin BI, Langer JS. Hopping Conductivity in Disordered Systems. Physical Review B. 1971;4(8):2612-2620.

[25] Miller A, Abrahams E. Impurity Conduction at Low Concentrations. Physical Review. 1960;120(3):745-755.

[26] Silva J, Simoes R, Lanceros-Mendez S, Vaia R. Applying complex network theory to the understanding of high-aspect-ratio carbon-filled composites. EPL (Europhysics Letters). 2011;93(3):37005.

[27] Connor MT, Roy S, Ezquerra TA, Baltá Calleja FJ. Broadband ac conductivity of conductor-polymer composites. Physical Review B. 1998;57(4):2286-2294.

[28] Grimaldi C, Ryser P, Strassler S. Gauge factor of thick-film resistors: Outcomes of the variable-range-hopping model. Journal of Applied Physics. 2000;88(7):4164-4169.

Figure Captions

Figure 1 – SEM images for MWCNT/SBS composites (C540 with 1% -above, and 4% wt -below) with two different magnification where is possible to observe both clusters dispersed in the polymer matrix and individual CNT. The small MWCNT clusters are observed for all composites, well distributed within the different polymer matrices.

Figure 2- Stress-Strain curves for different pure SBS.

Figure 3 – a) Stress-strain curves of SBS C540 filled with different contents of MWCNT and b) stress-strain curves for SBS/MWCNT composites with 1.95-3.68x10-2 volume fraction of MWCNT.

Figure 4 - Initial modulus for the different matrix as a function of the MWCNT contents. See also table 2 for the C540/MWCNT samples.

Figure 5 – a) Log-Linear plot of the electrical conductivity versus volume fraction of MWCNT for the SBS matrices and b) volume electrical conductivity of SBS/MWCNT nanocomposites versus volume fraction. The linear relations indicate that the electrical conductivity is due to hopping between the fillers.

Figure 6 – a) Variation of the electrical resistance ($\Delta R/R_0$) with strain ($\Delta L/L_0$) for the SBS/MWCNT composite (for 10 loading-unloading cycles. b) Gauge Factor, GF, as a function of strain for the C540 matrix with $1.95x10^{-2}$ volume fraction MWCNT.

Tables

Table 1 – Characteristics and denomination of the SBS used in this work.

SBS reference	C401	C411	C500	C540
Block copolymer structure	radial	radial	linear	linear
Styrene/Butadiene ratio	20/80	30/70	30/70	40/60

Table 2 – Mechanical properties of SBS C540/MWCNTs composites.

Sample	E	σ_{300}	σ_{900}	σ_{break}	ε_{break}
	MPa	MPa	MPa	MPa	%
0	43.9 ± 2.21	3.47 ± 0.17	8.55 ± 0.35	22.1 ± 1.13	1350 ± 75
$1.24x10^{-3}$	43.2 ± 2.20	3.31 ± 0.16	8.94 ± 0.39	23.6 ± 1.16	1344 ± 77
$4.96x10^{-3}$	54.4 ± 2.51	1.90 ± 0.10	10.19 ± 0.52	11.8 ± 0.61	970 ± 48
$9.87x10^{-3}$	50.2 ± 2.42	3.17 ± 0.16	10.39 ± 0.54	27.6 ± 1.36	1330 ± 75
$1.95x10^{-2}$	60.4 ± 3.11	3.47 ± 0.17	10.9 ± 0.57	16.96 ± 0.75	1157 ± 71
$3.83x10^{-2}$	114.0 ± 5.51	3.17 ± 0.16	6.63 ± 0.32	10.9 ± 0.53	1370 ± 76

Table 3. Percolation threshold and critical exponents calculated for the different SBS nanocomposites (R^2 is the coefficient of linear correlation).

C401				C411				C500			
Φ_c	t	R^2	δ_{max} (nm)	Φ_c	t	R^2	δ_{max} (nm)	Φ_c	t	R^2	δ_{max} (nm)
$9.18x10^{-3}$	~3	0.999	1.67	$2.22x10^{-3}$	~1	0.843	6.89	$1.47x10^{-3}$	~2	0.998	10.4

Figures

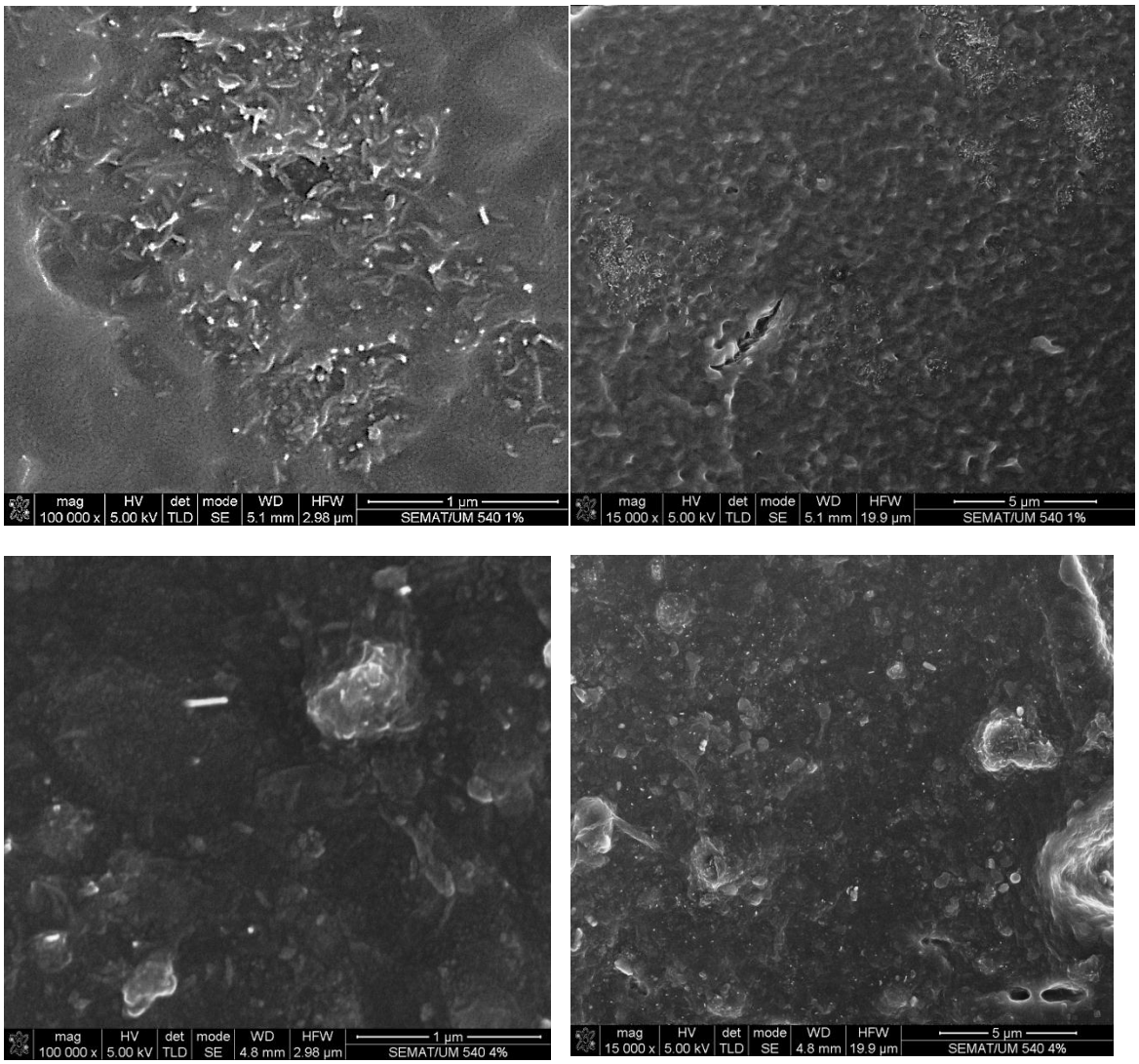

Figure 1 – SEM images for MWCNT/SBS composites (C540 with 1% -above, and 4% wt - below) with two different magnification where is possible to observe both clusters dispersed in the polymer matrix and individual CNT. The small MWCNT clusters are observed for all composites, well distributed within the different polymer matrices.

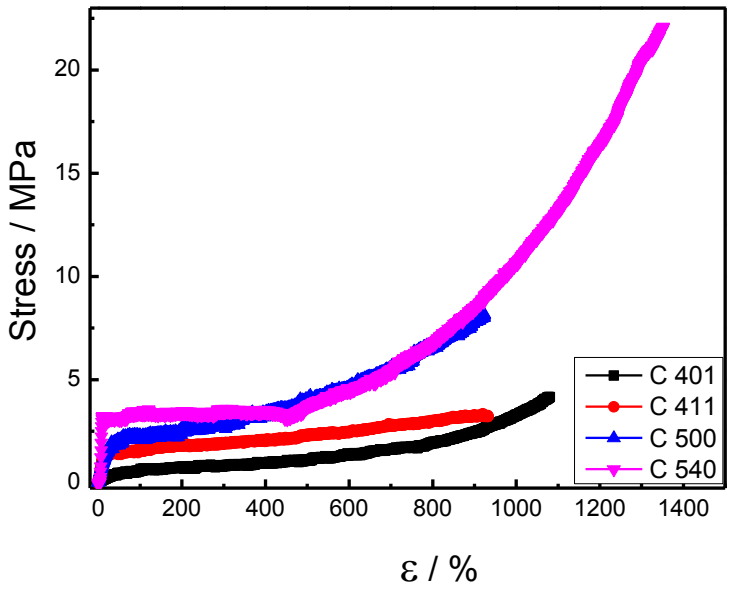

Figure 2- Stress-Strain curves for different pure SBS.

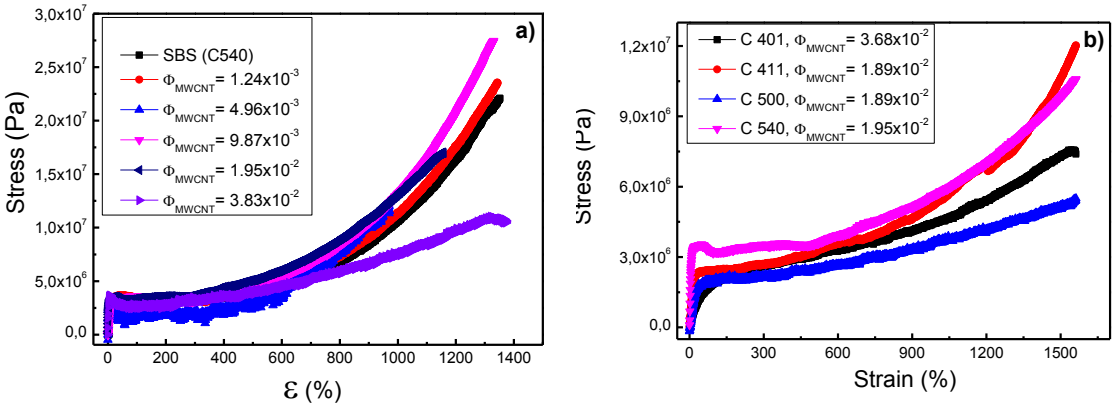

Figure 3 – a) Stress-strain curves of SBS C540 filled with different contents of MWCNT and b) stress-strain curves for SBS/MWCNT composites with 1.95-3.68x10-2 volume fraction of MWCNT.

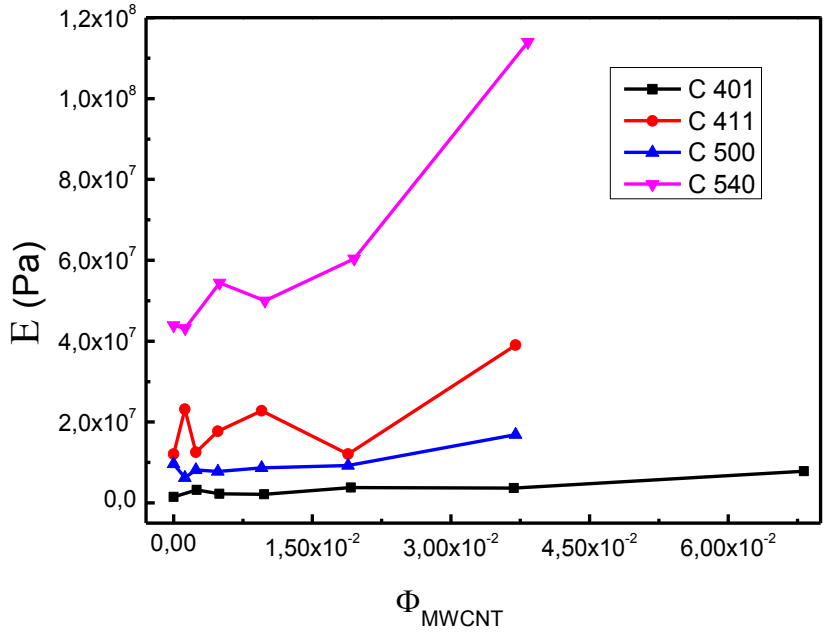

Figure 4 - Figure 4 - Initial modulus for the different matrix as a function of the MWCNT contents. See also table 2 for the C540/MWCNT samples.

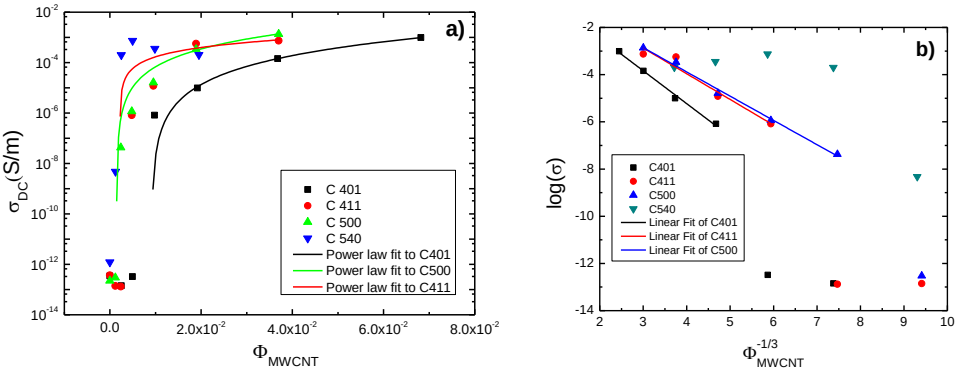

Figure 5 – a) Log-Linear plot of the electrical conductivity versus volume fraction of MWCNT for the SBS matrices and b) volume electrical conductivity of SBS/MWCNT nanocomposites versus volume fraction. The linear relations indicate that the electrical conductivity is due to hopping between the fillers.

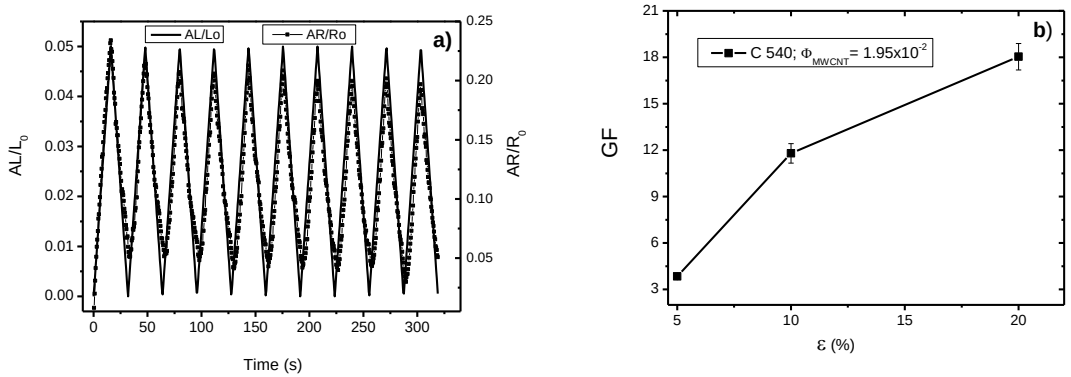

Figure 6 – a) Variation of the electrical resistance ($\Delta R/R_0$) with strain ($\Delta L/L_0$) for the SBS/MWCNT composite (for 10 loading-unloading cycles. b) Gauge Factor, GF, as a function of strain for the C540 matrix with $1.95x10^{-2}$ volume fraction MWCNT.